Chirality Changes in Carbon Nanotubes Studied with Near-Field Raman Spectroscopy

Neil Anderson,[†] Achim Hartschuh,[‡] and Lukas Novotny*,[†]

The Institute of Optics, University of Rochester, Rochester, New York 14627, and Department Chemie und Biochemie, Ludwig-Maximilians Universitaet Muenchen, Butenandtstrasse 11, 81377 Muenchen, Germany

ABSTRACT

We report on the direct visualization of chirality changes in carbon nanotubes by mapping local changes in resonant RBM phonon frequencies with an optical resolution of 40 nm using near-field Raman spectroscopy. We observe the transition from semiconducting-to-metal and metal-to-metal chiralities at the single nanotube level. Our experimental findings, based on detecting changes in resonant RBM frequencies, are complemented by measuring changes in the G-band frequency and line shape. In addition, we observe increased Raman scattering due to local defects associated with the structural transition. From our results, we determine the spatial extent of the transition region to be $L_{trans} \sim$ 40−100 nm.

In recent years, considerable interest has centered on the optical and electronic properties of single-walled carbon nanotubes (SWNTs). SWNTs are quasi-one-dimensional structures. Their formation is readily understood by visualizing how a single graphene sheet is rolled up into a cylindrical form. It is the departure from a single graphene layer and the introduction of periodic boundary conditions that provides carbon nanotubes with their unique optical and electronic properties. SWNTs can be either metallic or semiconducting depending on how the graphene sheet has been "rolled up". The structure of a carbon nanotube is assigned two integers (n,m). The graphene sheet is rolled up in such a way that a graphene lattice vector $\mathbf{C}_h = n\mathbf{a_1} + m\mathbf{a_2}$ becomes the circumference of the nanotube. The circumferential vector $\mathbf{C}_h$, which is typically denoted by the pair of integers (n,m), is called the chiral vector and uniquely defines the nanotube structure.[1]

Determining whether a carbon nanotube is conducting or nonconducting is crucial when considering their suitability for electronic or photonic device applications. Recent advances in our understanding of carbon nanotubes foresee potential application for specific types of nanotube structures as nanoscale diodes and rectifiers.[2−4] Such structures are known as intramolecular junctions (IMJs). An intramolecular junction is formed through structural defects, such as the formation of heptagon−pentagon pairs, that facilitate the growth of one chirality (n,m) to a different chirality (n',m').[5] Consequently, such a defect can give rise to either metal−metal, metal−semiconducting or semiconducting−metal transitions. The exploration of IMJs in carbon nanotubes is not confined to this Letter. The electronic properties of IMJs have been studied previously from both an experimental and theoretical perspective.[2,6,7] More recently, confocal Raman spectroscopy was used to highlight the existence of an IMJ in an ultralong single-walled carbon nanotube based on measuring the disappearance of one resonant RBM phonon and a change in the associated G-band frequency and line shape.[8]

Optical resonances in carbon nanotubes are excitonic in nature.[9] Resonance enhancement in the Raman cross-section is achieved by matching the incident laser energy to an optical transition E_{ii}. As a result, resonant Raman spectroscopy can be used to probe and acquire detailed structural information at the single nanotube level. The Raman modes important in determining and studying the presence of intramolecular junctions in carbon nanotubes are, namely: the radial breathing mode (RBM) (100−400 cm^{-1}),[10] defect-induced D-band (1300 cm^{-1}), which can be used to determine increase defect-related Raman scattering,[11] and the tangential stretching G-band ($\sim$1590 cm^{-1}).[12] The ability to directly measure the Raman shift of a resonant RBM phonon (ν_{RBM}) allows one to determine the diameter d_t and chirality (n,m)

---

* Corresponding author. E-mail: novotny@optics.rochester.edu.
† The Institute of Optics, University of Rochester.
‡ Department Chemie und Biochemie, Ludwig-Maximilians Universitaet Muenchen.

of the carbon nanotube using the following relations:[10,1]

$$\nu_{RBM} = \frac{A}{d_t} \qquad (1)$$

$$d_t = \frac{\sqrt{3}a_o}{\pi}\sqrt{n^2 + m^2 + nm} \qquad (2)$$

where $A = 248$ cm^{-1} × nm, a_o is the lattice constant of graphite ($a_o = 0.144$ nm), and (n,m) define the number of steps along the graphene basis vectors. A determination of whether a carbon nanotube is semiconducting or metallic based on detecting resonant RBM phonons can be supported by analyzing the frequency and line shape of the G-band. Semiconducting carbon nanotubes have a characteristic two-peak structure, where the lower frequency component is associated with vibrations along the cicumferential direction and the higher frequency component is attributed to vibrations along the nanotube axis, whereas metallic SWNTs have an additional feature on the low-energy side.[13] Defects in carbon nanotubes, such as changes in the carbon−carbon bonding and sidewall vacancies, are characterized by the presence of a vibrational line centered around 1300 cm^{-1}. For a change in chirality to occur a transformation in the carbon−carbon bonding in the nanotube sidewall must take place. Such structural changes can be caused by the formation of pentagon−heptagon "defect" pairs.[5] Therefore, localized disorder-induced (D-band) Raman scattering can also be observed at the IMJ region.

We define a "vibrational transition region", i.e., the IMJ junction, as that which gives rise to a local perturbation of phonon modes. The spatial extent over which a phonon is affected depends on the nature of the phonon mode and the nature of the defect. In this Letter, we report using near-field Raman spectroscopy, the observation of IMJs based on mapping resonant RBM phonon frequencies along spatially isolated SWNTs. The observed chirality changes based on shifts in the resonant RBM phonon frequencies are supported by our observation that the G-band frequency and line shape also changes around the junction. In addition, for some IMJs, we are able to measure significant changes in the strength of defect-induced (D-band) Raman scattering localized to the IMJ. From our measurements, we determine the length of the region with modified Raman characteristics caused by IMJs in SWNTs can range from 40 to 100 nm.

The SWNTs used in this study were grown by arc discharge using Ni/Y catalyst particles. The nanotubes were then purified to remove unwanted amorphous carbon and other residuals. Having been mixed in a solution of 1,2-dichloroethane, the carbon nanotubes were then dispersed onto a transparent glass coverslip. In combination with confocal Raman imaging, shear-force AFM imaging measurements were performed to locate spatially isolated SWNTs from SWNT bundles that are also present. Our experimental setup is based on an inverted optical microscope with an *x,y* scan stage for raster scanning a sample.[14] A laser beam, excitation energy 1.96 eV ($\lambda_{exc} = 632.8$ nm) and optical power = 300 μW, is reflected by a dichroic beam splitter

(BS) and focused on the sample surface using a high numerical aperture microscope objective (1.4 NA). A sharp gold tip is positioned in the focus of the laser beam and held at a constant height of 2 nm above the sample by means of a shear-force feedback mechanism.[15] To establish a strong field enhancement, we coupled the gold tip to the longitudinal field of a tightly focused Gaussian beam.[16] A near-field Raman image was recorded by raster-scanning the sample. The Raman scattered light was collected by the same microscope objective, transmitted by the dichroic BS, and detected using either a combination of bandpass filters and a single-photon counting avalanche photodiode (APD) or using a spectrograph equipped with a charged coupled device (CCD) cooled to −124 °C. Sharp gold tips with a diameter of 20−30 nm were produced by electrochemical etching in hydrochloric acid (HCl).

The combination of confocal Raman microscopy and spectroscopy was used initially to determine the location and presence of two spectrally distinct RBMs from the same sample area. A repeat scan was performed, this time with a sharp gold tip placed in the laser focus to provide a nanoscale map of the sample surface. In this way, it is possible to build vibrational maps of carbon nanotubes with ultrahigh spatial resolution.[14,17] A near-field Raman scattering image of an isolated SWNT exhibiting two spectrally distinct RBM frequencies is shown in Figure 1a, where the image contrast is provided by spectrally integrating over the G-band, along with the corresponding topographic image Figure 1b. The optical resolution provided by the gold tip was 40 nm. Shown in Figure 1c are a series of near-field Raman spectra acquired from the same SWNT. The local Raman spectrum was acquired by positioning the gold tip directly above the carbon nanotube. Over the upper portion of the nanotube, we detected a RBM frequency of 251 cm^{-1}. Using eq 1, we determined the nanotube diameter to be 0.99 nm. This RBM phonon frequency can be assigned to a semiconducting SWNT with diameter $d^{SC}_t = 0.94$ nm and structure (n,m) = (10,3), $E_{ii} = 1.98$ eV.[18] Over the lower portion of the same nanotube, we detected a RBM frequency of 192 cm^{-1}. Using eq 1, we determined the nanotube diameter to be 1.30 nm. The RBM phonon frequency can be assigned to a metallic SWNT with diameter $d^M_t = 1.25$ nm and (n,m) = (12,6) with $E_{ii} = 1.93$ eV or (n,m) = (13,4) with $E_{ii} = 1.94$ eV.[18] (The error associated with the experimentally determined phonon frequencies is ±3 cm^{-1}). Our assignments are based on the requirement that the RBM frequencies be resonant or near resonant with the excitation energy of 1.96 eV.[18]

Near-field Raman spectroscopy provides three methods with which to determine the existence and location of an intramolecular junction. The two optical methods are Raman microscopy and spectroscopy, respectively, which allow us to identify the location of a specific spectral signature. The third method at our disposal is shear-force AFM imaging and allows us to simultaneously map the surface topography. Therefore, in addition to the measured optical response, we used the simultaneously acquired topographic data to determine that a change in nanotube chirality has occurred, i.e., change in nanotube diameter. From the corresponding
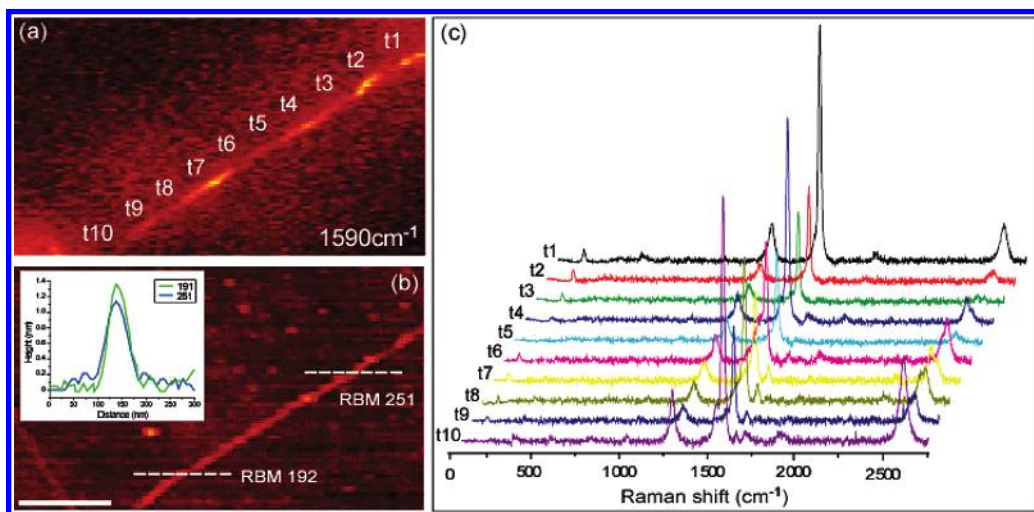
Figure 1. Near-field Raman imaging and spectroscopy: near-field Raman image (a) and corresponding topography image (b) of an isolated SWNT, where the optical resolution was determined to be 40 nm (fwhm). Also shown are a series of tip-enhanced Raman spectra (c) acquired along the length of the SWNT. From the recorded spectra, two resonant RBM phonons are detected. One RBM phonon frequency is detected at 251 cm^{-1}, from which we assign a semiconducting chirality. The second RBM phonon frequency recorded from the lower section of the SWNT is centered at 192 cm^{-1}, from which we assign a metallic chirality. See main text for details. The inset of (b) displays two cross-sectional profiles acquired from both the upper and lower sections, respectively, revealing that the expected diameter change occurs as the SWNT undergoes the transition from a semiconducting to metallic chirality. Scale bar denotes 200 nm and is valid for both (a) and (b).

topographic image shown in Figure 1b, we obtained two cross-sectional profiles from the carbon nanotube. The two cross-sectional profiles shown were acquired from where the two spectrally distinct RBMs frequencies were detected. From this measurement, we determined the nanotube diameter to be $d^{SC}_t = 1.1$ nm and $d^M_t = 1.4$ nm over the upper and lower sections of the nanotube, respectively. Nanotube diameters were found to be constant in the respective sections. The error associated with both these values is ±0.3 nm. As is clearly evident, both these values are in close agreement with the values determined using the measured RBM phonon frequencies and eq 1.

The ability to measure two spectrally distinct different RBM phonons on either side of an intramolecular junction has, to date, not been demonstrated experimentally. In Figure 2a, we show in detail the spectral evolution from one RBM phonon characteristic of a semiconducting nanotube, 251 cm^{-1}, $(n,m) = (10,3)$, into a RBM phonon characteristic of a metallic nanotube 192 cm^{-1}, $(n,m) = (12,6)$ or (13,4). (The Raman spectra displayed in Figure 2 were acquired from the SWNT shown in Figure 1.) As the gold tip was positioned along the nanotube, toward the transition region, the intensity of the RBM phonon along the semiconducting portion, I^{SC}_{RBM} decreases and then disappears. On the basis of the measured resonant RBM phonon frequencies, we determine, in that we can spatially locate a node in the RBM intensity, that the intramolecular junction affects the RBM phonons on a length scale of approximately 100 nm, i.e. the length of this transition region is greater than the spatial resolution (40 nm) of the experiment given by diameter of our gold tip, i.e., $L_{trans} > L_{tip}$. The absence of a RBM phonon at the intramolecular junction can therefore be the result of (1) a local RBM phonon that is not resonant with our excitation source or (2) the transition region does not support a RBM because of structural inhomogeneities. (Recently Vitali et al.[19] have

shown, using scanning tunneling microscopy (STM), that ultrashort segments of carbon nanotube approximately 3 nm in length do not support radial breathing modes and is consistent with our current findings.) After the junction, we detect a second RBM phonon resonant with our excitation source at 191 cm^{-1} and determine that this portion of the nanotube is metallic. Once again, we observe that the Raman intensity decreases along the nanotube and disappears completely at the nanotube end (t10), indicating that a significant structural change has occurred that no longer supports a RBM phonon in resonance with our excitation source, see Figure 2a. We believe this observation reflects the nature of termination point of the nanotube.

In addition to changes from a semiconducting to a metallic chirality based on resonant RBM frequencies, we also observed a change in the frequency and line shape of the G-band. The G-band in semiconducting carbon nanotubes exhibits two Lorentzian features, whereas metallic carbon nanotubes exhibit a line shape having a broad shoulder (G1) on the low-energy side of a Lorentzian (G2).[20,21] The evolution of the G-band line shape along the nanotube is shown in Figure 2b. Over the upper portion of the nanotube, a single Lorentzian is observed. Close to the transition region (t5), a low-energy peak, G1 ∼ 1550 cm^{-1}, appears and is present along the lower (metallic) portion of the nanotube (t6−t10), indicative of a metallic nanotube. The presentation of G-band spectra clearly reveals the transition from a line shape characteristic of a semiconducting to metallic structure and supports our claim for the existence of an intramolecular junction based on changes in the measured resonant RBM frequencies. We note that, while the metallic SWNT does not exhibit a strong broadened low-frequency G-band component, its metallic character is evident from the observed RBM frequency at 192 cm^{-1} and the resonance condition for laser excitation at 1.96 eV.[18] In addition, we
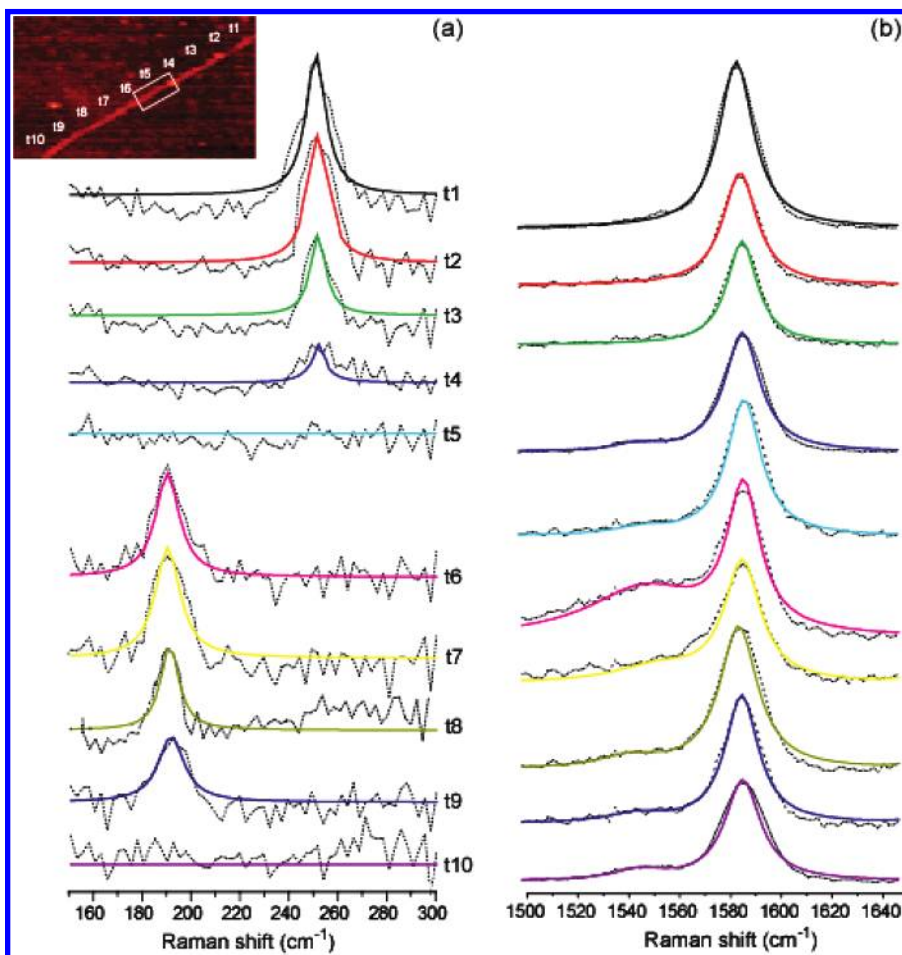
Figure 2. Near-field Raman spectra: series of near-field Raman spectra revealing the shift in the measured resonant RBM phonon frequency (a) and G-band frequency and line shape (b). The inset of (a) displays the topographic image of the carbon nanotube studied, indicating where the Raman spectra were acquired and the spatial extent of the intramolecular junction (IMJ), as indicated by the boxed region. As (a) shows, we record a shift in the measured RBM phonon frequency along the length of the carbon nanotube, revealing a clear transition from a semiconducting chirality [ν_{RBM} = 251 cm^{-1}, (n,m) = (10,3)] to a metallic chirality [ν_{RBM} = 192 cm^{-1}, (n,m) = (12,6) or (13,4)]. In addition to detecting a shift in the RBM phonon mode, (b) reveals a transformation of the G-band from a single Lorentzian line shape, characteristic of a semiconducting SWNT to a double peak line shape characteristic of a metallic SWNT.

note that, within our spectral detection window 700−1000 nm, no photoluminescence localized to the semiconducting portion of the SWNT was observed.[22]

It is known that the arrangement of carbon atoms in the nanotube sidewall must deviate from the typical hexagonal structure for intramolecular junctions to form. As a result, the translational symmetry of the SWNT structure is broken, which can manifest itself as a defect-induced peak in the measured Raman spectrum. One possible arrangement is the formation of pentagon−heptagon "defect" pairs.[23] Therefore, in addition to detecting a chirality change based upon measuring variations in resonant RBM frequencies and G-band line shape, increased defect Raman scattering, localized to the transition region, can also be present.

To reveal the change in D-band scattering that occurs over the spatial extent of the junction region L_{trans}, we present in Figure 3 a plot displaying the variation in the integrated Raman intensity of the defect-induced Raman peak and RBM frequency along the SWNT shown in Figure 1. The integrated D-band intensity was calculated with an accuracy of r^2 = 0.98. As Figure 3 clearly shows, a pronounced
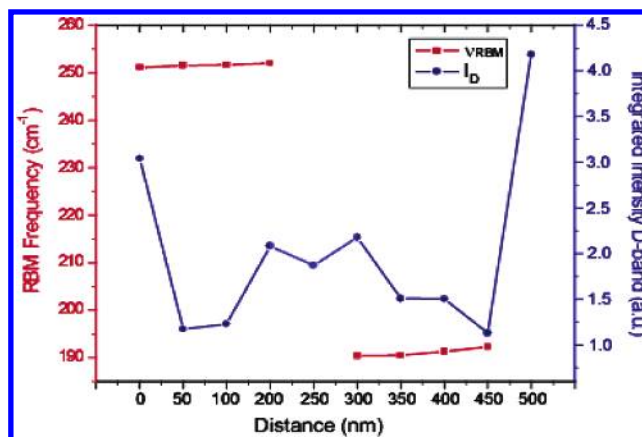

Figure 3. Defect-induced Raman scattering localized at an intramolecular junction: a plot of RBM frequency and integrated D-band Raman intensity as a function of position along the carbon nanotube shown in Figure 1. The plot reveals a correlation between increased D-band scattering and the spatial location of the transition region, defined by the absence of a resonant RBM phonon.

increase in D-band scattering occurs over the region bridging the semiconducting and metallic portions of the SWNT. We
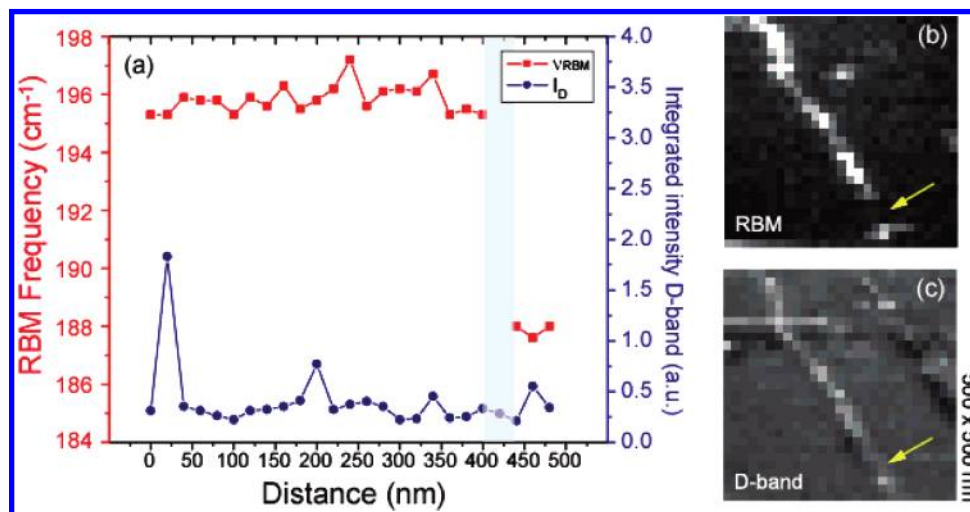
Figure 4. Variation in resonant RBM and D-band scattering along a SWNT. (a) Plot of the peak position of two resonant RBMs and D-band Raman scattering intensity along a SWNT. Two spectrally distinct RBM phonon frequencies can be detected. The first RBM has a phonon frequency $\nu_{\text{RBM}} \sim 196$ cm^{-1}, $(n,m) = (14,2)$ having metallic character and is measured along a region of 400 nm of the SWNT. There exists a gap where no RBM phonon in resonance with our laser could be detected. This region defines the spatial extent of the IMJ and is indicated by the arrows in the near-field Raman images shown in (b) and (c). The spatial extent of the IMJ for this SWNT was L_{trans} ~ 40 nm and is twice the size of the spatial resolution provided by the gold tip used, $[\Delta x = 20$ nm (fwhm)]. A second RBM was detected at the end of the SWNT and has a phonon frequency $\nu_{\text{RBM}} \sim 188$ cm^{-1}, $(n,m) = (12,6)$ having metallic character. The variation in D-band Raman scattering intensity reveals that no increase exists at the junction region, see (c). The near-field Raman image for the RBM shown in (b) reveals that a gap between the two regions of the SWNT, where the RBM phonons can be measured is easily resolved.

believe that the presence of D-band scattering reflects the intrinsic properties of the SWNT studied and is not related to the presence of amorphous carbon or other carbon-based residuals as the SWNTs used were purified after growth. Although we measure defect-induced Raman scattering along the entire length of the nanotube, and it is consistent with previous near-field Raman studies of arc-discharge carbon nanotubes,[14,17] over the portion (t4−t6) where the intramolecular junction is located, we observe increased D-band scattering on a length scale comparable to L_{trans}. That is, L_{trans} $\sim L_{\text{D}} \sim 100$ nm.

Intramolecular junctions are typically associated with changes from semiconducting-to-metallic chiralities (and vice versa). However, semiconducting-to-semiconducting and metal-to-metal junctions also occur.[2] In Figure 4a, we display the variation in RBM phonon frequency and D-band Raman intensity along a different SWNT. Parts b and c of Figure 4 show near-field Raman images where the image contrast is provided by spectrally integrating over the RBM and D-band Raman lines. This data set was acquired using a different gold tip where the optical resolution provided by the gold tip was $L_{\text{tip}} \sim 20$ nm (fwhm). From Figure 4a, a clear shift in resonant RBM phonon frequency is measured along the SWNT. Over the first 400 nm of the SWNT shown in Figure 4b, we detected a RBM phonon frequency $\nu_{\text{RBM}} \sim 196$ cm^{-1}, $(n,m) = (14,2)$, $E_{\text{ii}} = 1.94$ eV, having metallic character.[18] Then, over a 40 nm section of the SWNT, no RBM phonon is detected. This can be seen as a gap in the near-field RBM image shown in Figure 4b. This node allows us to determine that the spatial extent of the IMJ is $L_{\text{trans}} \sim 40$ nm, where once again $L_{\text{trans}} > L_{\text{tip}}$ revealing that the spatial resolution in our experiment does not limit the measurement. Over the last 40 nm of the SWNT, we detect an RBM phonon frequency $\nu_{\text{RBM}} \sim 188$ cm^{-1}, $(n,m) = (12,6)$, $E_{\text{ii}} = 1.93$ eV,

having metallic character.[18] As Figure 4a reveals, increased defect-induced Raman scattering could not be localized to the transition region.

In summary, we have shown, using near-field Raman spectroscopy, chirality changes based on mapping two resonant RBM phonon frequencies along spatially isolated SWNTs. In doing so we have mapped the transition from both semiconducting-to-metal and metal-to-metal chiralities at the single nanotube level. The observed variations based on detecting resonant RBM phonon frequencies are supported by variations in G-band frequency and line shape. In both cases, we determine the spatial extent of the transition region to be $L_{\text{trans}} \sim 40-100$ nm.

References

(1) Reich, S.; Thomsen, C.; Maultzsch, J. *Carbon Nanotubes: Basic Concepts and Physical Properties*, Wiley-VCH: Weinheim, 2004.
(2) Yao, Z.; Postma, H. W. Ch.; Balents, L.; Dekker, C. *Nature* **1991**, *402*, 273−276.
(3) McEuen, P. *Nature* **1998**, *393*, 15−17.
(4) Baughman, R.H.; Zakhidov, A. A.; de Heer, W. A. *Science* **2002**, *297*, 787−792.
(5) Iijima, S.; Ichihashi, T.; Ando, Y. *Nature* **1992**, *356*, 776−778.
(6) Chico, L.; Crespi, V. H.; Benedict, L. X.; Louie, S. G.; Cohen, M. L. *Phys. Rev. Lett.* **1996**, *76*, 971−974.
(7) Li, Y.; Ravaioli, U.; Rotkin, S. V. *Phys. Rev. B* **2006**, *73*, 035415.
(8) Doorn, S. K.; O'Connell, M. J.; Zheng, L.; Zhu, Y. T.; Huang, S.; Liu, J. *Phys. Rev. Lett.* **2005**, *94*, 016802.

(9) Wang, F.; Dukovic, G.; Brus, L. E.; Heinz, T. F. *Science* **2005**, *308*, 838−841.

(10) Jorio, A.; Saito, R.; Hafner, J. H.; Lieber, C. M.; Hunter, M.; McClure, T.; Dresselhaus, G.; Dresselhaus, M. S. *Phys. Rev. Lett.* **2001**, *86*, 1118−1121.

(11) Maultzsch, J.; Reich, S.; Thomsen, C. *Phys. Rev. B* **2001**, *64*, 121407.

(12) Jorio, A.; Souza Filho, A. G.; Dresselhaus, G.; Dresselhaus, M. S.; Swan, A. K.; Unlu, M. S.; Goldberg, B. B.; Pimenta, M. A.; Hafner, J. H.; Lieber, C. M.; Saito, R. *Phys. Rev. B* **2002**, *65*, 155412.

(13) Dresselahaus, M. S.; Dresselhaus, G.; Jorio, A.; Souza Filho, A. G.; Saito, R. *Carbon* **2002**, *40*, 2043−2061.

(14) Hartschuh, A.; Sánchez, E. J.; Xie, X. S.; Novotny, L. *Phys. Rev. Lett.* **2003**, *90*, 095503.

(15) Karrai, K.; Grober, R. D. *Appl. Phys. Lett.* **1995**, *66*, 1842−1844.

(16) Hartschuh, A.; Anderson, N.; Novotny, L. *J. Microsc.* **2003**, *210*, 234−240.

(17) Anderson, N.; Hartschuh, A.; Cronin, S.; Novotny, L. *J. Am. Chem. Soc.* **2005**, *127*, 2533−2537.

(18) Maultszch, J.; Telg, H.; Reich, S.; Thomsen, C. *Phys. Rev. B* **2005**, *72*, 205438.

(19) Vitali, L.; Burghard, M.; Schneider, M. A.; Liu, L.; Wu, S. Y.; Jayanthi, C. S.; Kern, K. *Phys. Rev. Lett.* **2004**, *93*, 136103.

(20) Oron-Carl, M.; Hennrich, F.; Kappes, M. M.; Lohneysen, H. V.; Krupke, R. *Nano Lett.* **2005**, *5*, 1761−1767.

(21) Brown, S. D. M.; Corio, P.; Marucci, A.; Pimenta, M. A.; Dresselhaus, M. S.; Dresselhaus, G. *Phys. Rev. B* **2000**, *61*, 7734−7742.

(22) Hartschuh, A.; Qian, H.; Meixner, A.J.; Anderson, N.; Novotny, L. *Nano Lett.* **2005**, *5*, 2310−2313.

(23) Saito, R.; Dresselhaus, G.; Dresselhaus, M. S. *Phys. Rev. B* **1996**, *53*, 2044−2050.